Concentration-Tunable Liquid Graphene Oxide Magneto-Optical Sensor for Smart Grid Current Monitoring

Junyu Cheng[1]

202330411421@mail.scut.edu.cn[1]

School of Physics and Optoelectronics, South China University of Technology, Guangzhou, China

Abstract. Current sensors based on solid-state materials often suffer from magnetic saturation and stress-induced birefringence, limiting their performance in high-current applications. To address these issues, this paper proposes a tunable liquid-phase magneto-optical sensing scheme utilizing the Faraday effect in Graphene Oxide (GO) dispersions. A transmission-mode detection system utilizing a "Differential Baseline Subtraction" algorithm was constructed to isolate intrinsic magneto-optical characteristics from parasitic solvent interferences. Experimental results demonstrate a giant specific Verdet constant of $1.72 \times 10^4 \mathrm{rad}/(\mathrm{T} \cdot \mathrm{m})$ in the ultra-dilute regime, confirming superior intrinsic efficiency. Through a comprehensive trade-off analysis between sensitivity and stability, 0.008 wt% was identified as the optimal engineering concentration. This configuration achieves a sensitivity of -0.00391 mV/mT and high linearity ($R^2 > 0.98$), while suppressing hysteresis error to 6.57%, thereby effectively mitigating the instability observed at the lower concentrations. Furthermore, the mechanisms of "Concentration Quenching" and "Structural Locking" are elucidated to explain non-linear responses at higher densities. This research validates the feasibility of GO dispersions for high-fidelity, range-configurable current monitoring in Smart Grids.

Keywords: Optical Current Sensor; Graphene Oxide; Faraday Effect; Smart Grid

1 Introduction

With the evolution of the "Smart Grid" and "Transparent Power Grids," precise sensing of "High-Current" has become a core prerequisite for system control and protection [1]. However, traditional "Current Transformers" (CTs) suffer from severe intrinsic limitations, including excessive physical footprint, risk of protection failure due to "Magnetic Saturation", and inability to meet the broadband measurement demands of "HVDC" systems [2, 3]. Consequently, Optical Current Sensors (OCS) based on the "Faraday Effect" have emerged as ideal alternatives due to their superior insulation and interference immunity, despite the unresolved engineering contradictions in current mainstream technologies.

Existing OCS technologies face severe engineering challenges: all-fiber sensors are limited by "Linear Birefringence," making them susceptible to thermal stress and vibration [2-5], while bulk crystal sensors suffer from significant temperature drift of the "Verdet Constant" and fixed measurement ranges due to solid packaging. Although "Magnetic Fluid" offers liquid-state

ICMEEA 2026, April 24-26, Singapore, Singapore

DOI 10.4108/eai.24-4-2026.2364894

advantages, it is plagued by nanoparticle "Aggregation," sedimentation, and poor optical transmission [6].

To address these bottlenecks, GO offers a breakthrough with its giant "Shape Anisotropy" and excellent water dispersibility [7]. GO not only exhibits high magneto-optical sensitivity in its liquid crystal phase but also theoretically eliminates stress-induced birefringence. This paper proposes a novel liquid current sensing scheme based on the "Faraday Effect" of GO solution, bridging the gap in industrial frequency high-current monitoring. Leveraging unique "Concentration Tunability," this approach overcomes the fixed sensitivity of solid crystals, enabling flexible adaptation to a wide dynamic range—from amperes to kilo-amperes—simply by adjusting solution concentration [8].

The research logic is organized as follows: First, the preparation of GO is optimized to establish a quantitative mapping between solution concentration and the "Verdet Constant." Second, a transmission optical setup is constructed to physically verify the elimination of stress-induced birefringence by the liquid medium. Subsequently, linearity and response characteristics are evaluated under industrial frequency magnetic fields using a Helmholtz coil platform. Finally, the physical mechanisms of "Concentration Quenching" and "Structural Locking" are elucidated to explain the response characteristics. Based on these insights, a comprehensive trade-off analysis between sensitivity and dynamic stability is conducted to determine the optimal engineering operating point for high-current monitoring.

2 Theoretical Basis and Sensing Principles

2.1 Static Magneto-Optical Coupling Model of GO Dispersion

Adopting a transmission-mode architecture, the optical beam penetrates the GO dispersion phase and background media (solvent and cuvette). Under the steady magnetic flux density B generated by a Helmholtz coil, the total static rotation angle θ_{total} follows the superposition principle of the "Faraday Effect":

$$\theta_{total} = \theta_{GO} + \theta_{bg} = \left(V_{GO} + V_{bg}\right) \cdot L \cdot B \quad (1)$$

Where V_{GO} and V_{bg} denote the effective "Verdet Constant" of the GO and background media, respectively, and L is the effective optical path length. This model indicates a strict linear relationship between θ_{total} and magnetic field intensity B.

2.2 Photoelectric Conversion and DC Transfer Function

A "polarizer-sample-analyzer" detection link is established, introducing an optical "Bias Angle" φ to set the static operating point. According to Malus's Law, the received DC light intensity I is given by:

$$I = I_0 \sin^2(\varphi + \theta_{total}) \quad (2)$$

Optical signals are captured by a silicon photodetector (Thorlabs DET36A2) with a responsivity $\Re_\lambda = 0.114$A/W at 450 nm. The photocurrent is converted into voltage U_{DC} via a load resistor R_L. The static "magneto-optical-electrical" transfer function is derived as:

$$U_{DC} = \Re_\lambda \cdot R_L \cdot I_0 \sin^2\left(\varphi + \left(V_{GO} + V_{bg}\right) \cdot L \cdot B\right) \quad (3)$$

2.3 Differential Slope Method and Parasitic Effect Decoupling

To precisely extract intrinsic GO characteristics, a multi-point scanning and linear fitting strategy is employed. The voltage responses of the pure solvent control and GO dispersion are measured under current excitation (-5 A to 5 A), yielding the background slope K_{bg} and total slope K_{total} via linear regression. Under small-angle approximation ($\theta \ll 1\ rad$) and optimal bias angle ($\varphi = \frac{10}{3}°$), the net sensitivity K_{GO} is decoupled using the "Differential Slope Method" based on the superposition principle:

$$K_{GO} = K_{total} - K_{bg} \tag{4}$$

This approach effectively eliminates parasitic magneto-optical interference from the cuvette and solvent, validating the sensor's linearity for wide-range monitoring through R^2 verification.

3 Design and Construction of GO Magneto-Optical Sensing System

3.1 Overall System Architecture

A magneto-optical detection system based on coaxial line-of-sight transmission was constructed (as shown in Fig. 1), with the optical path strictly aligned along the central axis of the rail. The measurement signal is generated by a 650 nm red semiconductor laser driven by a "Constant Current Source" to ensure power stability. The beam is first polarized by a Glan–Taylor prism, then traverses the GO cuvette placed at the magnetic center. The transmitted light, carrying magnetic-field-induced modulation, is analyzed by a second Glan–Taylor prism before detection with a Thorlabs DET36A2 photodetector. Finally, the photoelectric-converted voltage signal is acquired by a high-precision digital multimeter, which optimizes the sampling integration time to suppress power frequency interference and achieve quantized acquisition of millivolt-level weak magneto-optical signals.

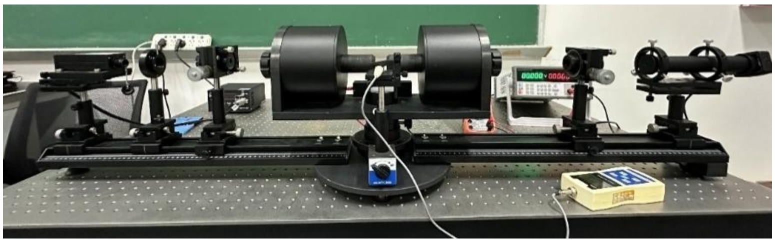

Fig. 1. Experimental apparatus

3.2 Magnetic Field Generation and Excitation Calibration

A "Helmholtz Coil" is selected as the magnetic source to ensure the uniformity of magnetic flux density B along the optical path, satisfying the linear integration prerequisite of the Faraday effect. The excitation system is driven by a programmable DC power supply, where the "Constant Current" mode effectively compensates for load drift caused by coil heating, as verified by the excellent long-term stability observed during a 30-minute continuous test.
To address the non-linearity in the $B - I$ relationship caused by core "Magnetic Saturation" at high currents, a "3rd-order Polynomial Model" is applied for regression analysis over the 0-5 A range:

$$B = 0.3968 \cdot I^3 - 16.8865 \cdot I^2 + 170.7152 \cdot I + 5.4185 \tag{5}$$

The fitting result yields a coefficient of determination $R^2 = 0.9998$, confirming that the model accurately reconstructs the excitation characteristics and ensures the precision of subsequent Verdet constant calculations. Fig. 2 illustrates the mapping relationship between excitation current (I) and central magnetic flux density (B).

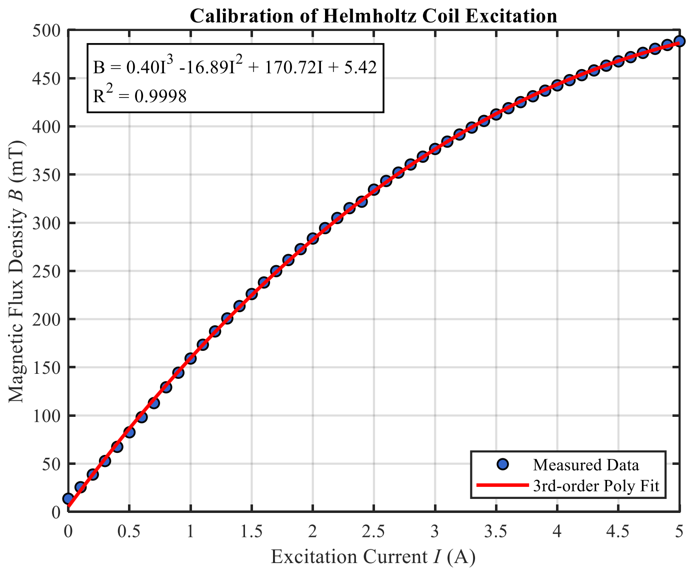

Fig. 2. B-I Characteristic Calibration and Nonlinear Fitting of the Helmholtz Coil Excitation System

3.3 Design and Debugging of Optical Detection Unit

3.3.1 Polarization Modulation and Static Operating Point Optimization

To detect weak signals from GO, the system abandons the traditional 45° bias in favor of a "Near-extinction Bias Strategy". The analyzer is rotated by $\varphi = \frac{10}{3}°$ from the orthogonal position to set the static working point (Q-point), based on two engineering considerations:

1. Enhancement of SNR and Modulation Depth: Unlike the 45° bias where high background intensity risks saturating the preamplifier, the near-extinction region suppresses static background and significantly boosts modulation depth ($\Delta I / I_{base}$), ensuring the detector operates in its optimal linear region.

2. Magnetic Field Direction Discrimination: At complete extinction (0°), the output intensity $I \propto \theta^2$ results in polarity loss. Introducing a small bias φ yields an approximation $I \propto (\varphi + \theta)^2 \approx \varphi^2 + 2\varphi\theta$ via Malus's Law. The linear cross-term $2\varphi\theta$ preserves sign information, enabling accurate demodulation of the optical rotation direction.

3.3.2 Sensor Structure and Optical Shielding

A standard quartz cuvette with an optical path $L = 10$mm is selected as the sensing core. This design represents an optimal trade-off between "magneto-optical gain" ($\theta \propto L$) and "scattering loss," preventing exponential attenuation of transmission caused by long path lengths in turbid media. Furthermore, the optical alignment follows the "coaxial line-of-sight" principle, ensuring the laser beam parallels the magnetic field lines of the Helmholtz coil. A matte black shield is installed to suppress environmental noise below the detector's "Noise Equivalent Power" (NEP), ensuring voltage fluctuations originate solely from magneto-optical modulation.

3.4 Material Preparation and Concentration Threshold Screening

Glycerol and distilled water (1:1 v/v) are selected as the composite solvent for GO to inhibit "Brownian Motion" and enhance sedimentation stability via high viscosity. To determine the optimal sensing operating point, three mass concentrations (0.0029%, 0.005%, and 0.008%) were evaluated. Results indicate that lower concentrations (0.0029% and 0.005%) were limited by "Signal-to-Noise Ratio" (SNR) bottlenecks, where the magnetic torque failed to overcome Brownian motion, resulting in modulation depths below the "Limit of Detection" (LOD). In contrast, the 0.008% sample successfully balanced optical transmission with the effective Verdet constant, enabling linear signal demodulation. Consequently, subsequent performance evaluations are based on the 0.008% concentration.

3.5 Experimental Procedures and Data Acquisition Scheme

To eliminate stray light and intrinsic system bias, a synchronous baseline subtraction algorithm is employed. First, the background response curve (Baseline) of the pure solvent is mapped over the full excitation range , followed by the measurement of the 0.008% GO dispersion under identical conditions. Data processing adheres to the "co-directional mapping subtraction" principle, subtracting the baseline data from the GO response for corresponding ascending and descending phases ($5A \rightarrow -5A$). This physically decouples system errors induced by core remanence and optical drift, ensuring the extracted ΔV curve purely reflects the magneto-optical contribution of the GO medium.

4 Experimental Results and Analysis

4.1 Data Preprocessing and Decoupling

This chapter aims to extract physically meaningful quantities from the raw photoelectric response. Given the nonlinear excitation, intensity mapping, and parasitic fluid effects, the data processing workflow is established as follows: First, the input current is corrected for "Magnetic Saturation" via the 3rd-order transfer function to reconstruct the true magnetic field. Second, absorption-induced signal attenuation is eliminated using Malus's law inversion and "Self-referenced Normalization". Finally, the "Differential Baseline Subtraction" algorithm is introduced to isolate the background solvent interference for extracting the intrinsic properties of GO.

4.1.1 Nonlinear Correction of Excitation Field

To address the nonlinearity of the Helmholtz coil at high currents, the excitation current sequence I is mapped point-by-point to the true central magnetic flux density B using the model calibrated in Section 3.2:

$$B = 0.3968 \cdot I^3 - 16.8865 \cdot I^2 + 170.7152 \cdot I + 5.4185 \quad (5)$$

This step physically corrects core magnetization errors, ensuring that subsequent magneto-optical analysis is based on the true magnetic field benchmark (Ground Truth).

4.1.2 Normalized Inversion of Physical Deflection Angle

To eliminate transmittance attenuation caused by the dark GO medium, a physical inversion model based on "Self-referenced Normalization" is constructed:

$$\theta_{GO} = arcsin\left(sin\varphi \cdot \sqrt{\frac{U_{out}}{U_{bias}}}\right) - \varphi \quad (6)$$

U_{out} is the measured voltage, U_{bias} is the bias voltage under zero excitation for the same experimental group. $\varphi = \frac{10}{3}^{\circ}$. This algorithm eliminates the common-mode attenuation factor T via voltage ratio calculation, ensuring the demodulated θ_{GO} purely reflects the magneto-optical rotation effect.

4.1.3 Baseline Drift and Background Noise Subtraction

Liquid sensing systems are subject to common-mode interference from the environment and non-target media: the glycerol/water matrix and quartz walls exhibit significant "Parasitic Faraday Effect" under strong magnetic fields, while laser thermal effects induce DC "Zero Drift". To eliminate systematic deviations, a "Differential Baseline Subtraction" algorithm is introduced based on the superposition principle. Specifically, the total response $\theta_{total}(B)$ of the GO dispersion is synchronously subtracted by the pure solvent background baseline $\theta_{bg}(B)$:

$$\theta_{GO}(B) = \theta_{total}(B) - \theta_{bg}(B) \quad (7)$$

As shown in Fig.3, the response slope of the 0.0029% GO dispersion is notably lower than that of the pure solvent baseline, intuitively revealing the "Negative Magneto-optical Effect" of GO relative to the solvent. By extracting the net response curve with a negative slope, this algorithm effectively isolates parasitic interference and low-frequency common-mode noise, establishing a precise data foundation for calibrating the intrinsic Verdet constant.

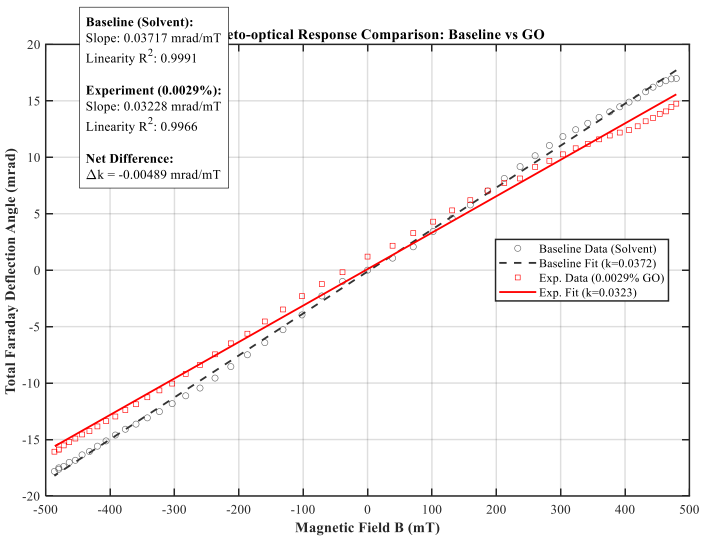

Fig. 3. Fitting Comparison of $\theta_{total} - B$ between 0.0029% GO Dispersion and Pure Solvent Baseline

4.2 Engineering Optimization of Sensing Characteristics: Trade-off between Signal Strength and SNR

4.2.1 Concentration Dependence of Macro Signal Gain

To determine optimal operating parameters, the differential response $\Delta V - B$ (defined as $\Delta V = U_{exp}$-U_{ctrl}) was evaluated for concentrations of 0.0029%, 0.005%, and 0.008%, focusing on "Sensitivity," "Linearity," and "Hysteresis Error." Experimental data (Table 1 and Fig.4) reveal the following evolution patterns:

Table 1. Comparison of sensing performance parameters with different GO concentrations

Concentration	Sweep	Slope(mV/mT)	Linearity R^2	Max Gap (mV)	Hysteresis (%)
0.0029%	Down	-0.00147	0.8582	1.37	34.08
	Up	-0.00147	0.4473		
0.005%	Down	-0.00333	0.9898	0.4200	5.99
	Up	-0.00214	0.3798		
0.008%	Down	-0.00391	0.9846	0.5900	6.57
	Up	-0.00254	0.3481		

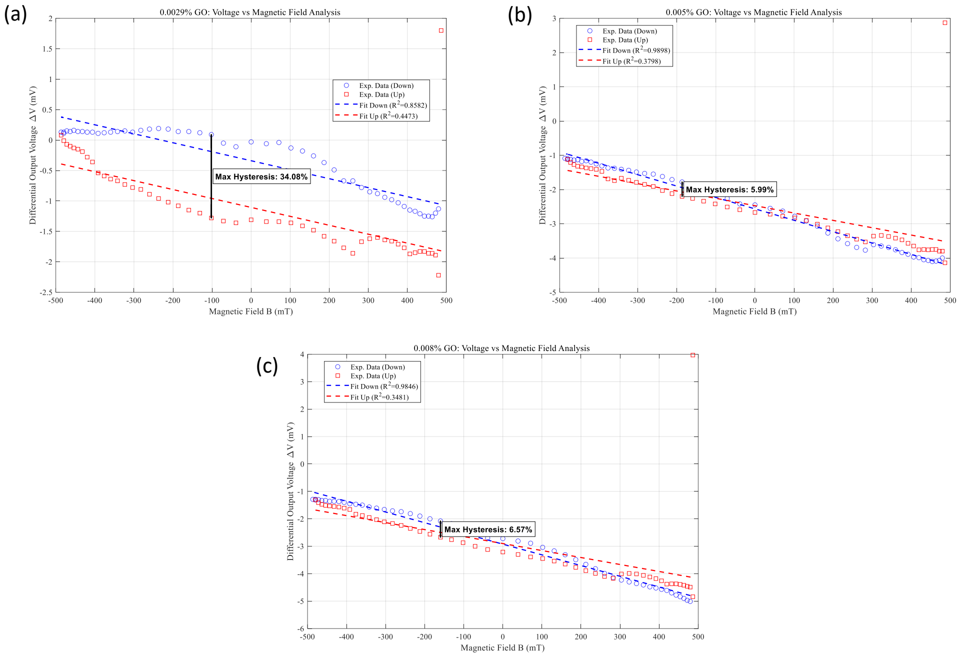

Fig. 4. $\Delta V - B$ Fitting Comparison at Three Concentrations

1.Gain Effect of Voltage Sensitivity: Sensitivity increases significantly with concentration. The low-concentration group (0.0029%) exhibits a weak sensitivity of only -0.00147 mV/mT due to insufficient active material, which results in poor linearity ($R^2 = 0.8582$) as a result of high noise susceptibility. The medium group (0.005%) doubles the sensitivity to -0.00333 mV/mT with improved linearity of 0.9898. The high-concentration group (0.008%) delivers the strongest output with a sensitivity of -0.00391mV/mT (approx. 2.66 times that of the low group) while maintaining excellent linearity ($R^2 = 0.9846$), demonstrating the enhancement of macro signals via the "collective effect".

2.Trade-off between Dynamic Hysteresis and Stability: he low-concentration group shows "engineering instability" with a maximum voltage gap of 1.3700mV and a staggering hysteresis error of 34.08% ,confirming poor magnetic orientation recovery dominated by Brownian motion. In contrast, the 0.005% group exhibits the minimum hysteresis (5.99%), while the 0.008% group shows a slight increase to 6.57% (max gap 0.5900mV), both indicating superior reversibility.

3.Final Determination of Engineering Operating Point: .008% is selected as the optimal operating point. Although the 0.005% group holds a marginal advantage in hysteresis (better by approx. 0.58%)， the 0.008% group yields a significant gain in sensitivity (increased by approx. 18%). Higher sensitivity translates to a superior "Signal-to-Noise Ratio" (SNR), while the hysteresis difference of less than 1% remains controllable. Thus, 0.008% achieves the best balance between "high SNR" and "manageable error."

4.2.2 Analysis of Static Extinction and Zero Offset

Under zero magnetic field (excitation current $I = 0A$), a negative "Initial Voltage Offset" is observed across all concentration groups relative to the pure solvent benchmark ($U_{ctrl} = 6.77\text{mV}$). Measurements indicate that the low concentration (0.0029%) exhibits a negligible offset of -0.03mV (attenuation $< 0.5\%$), implying near transparency, whereas the medium (0.005%) and high (0.008%) concentrations show significantly increased offsets of -2.45mV (attenuation 36.2%) and -2.72mV (attenuation 40.2%), respectively.
This phenomenon adheres to the "Beer-Lambert Law," confirming that the offset originates from intrinsic material "Static Extinction" or "Optical Damping," rather than circuit "Zero Drift". From an engineering perspective, this constant "DC Component" does not affect dynamic sensitivity and can be fully eliminated via hardware "Bridge Balancing" or software "Initial Taring". The conclusion affirms that the strategy of trading calibratable static loss for maximum dynamic gain in the 0.008% group is both rational and necessary.

4.3 Physical Intrinsic Magneto-Optical Response: Concentration Quenching and Monomer Mechanism

This section investigates the microscopic mechanisms based on the normalized net deflection angle θ_{GO}.

4.3.1 Monomer Free Response Mechanism in Ultra-Dilute Limit

At the ultra-dilute concentration of 0.0029%, the GO dispersion exhibits peak intrinsic sensitivity and symmetry (Down slope: -0.0050, $R^2 = 0.8693$; Up slope: -0.0052, $R^2 = 0.8043$). This highly linear response indicates that nanosheets are in a "quasi-free suspension state," where interlayer magnetic dipole interactions and steric hindrance are negligible, allowing local magnetic moments to align with the field in real-time, reflecting a typical monomeric magnetic response. Based on the Faraday formula $\theta_{GO} = V \cdot B \cdot L$ ($L = 10\text{mm}$), the Verdet constant is calculated as approx. $0.50\text{rad}/(\text{T} \cdot \text{m})$, with a specific Verdet constant reaching $1.72 \times 10^4 \text{rad}/(\text{T} \cdot \text{m})$. This value, two orders of magnitude higher than traditional TGG crystals, verifies the ultra-high magneto-optical efficiency derived from its unique topological electronic structure in the ultra-dilute state. Fig.5 is the linear fitting analysis of the intrinsic magneto-optical response (θ_{GO}) versus magnetic flux density (B) at a concentration of 0.0029%.

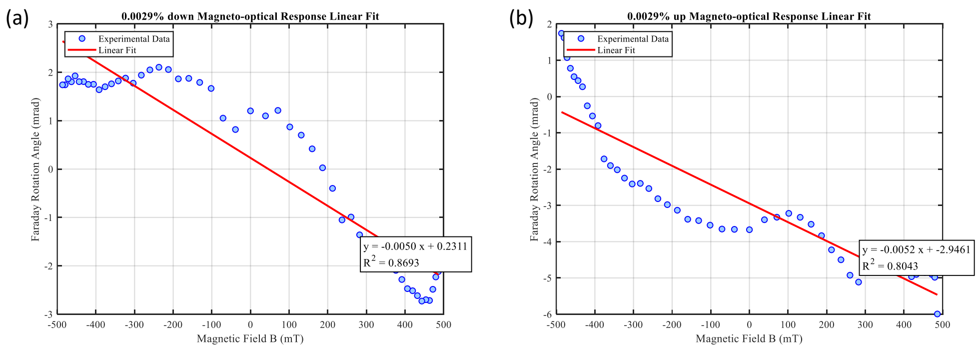

Fig. 5. Fitting Comparison of $\theta_{GO} - B$ at 0.0029%

4.3.2 Concentration Quenching and Structural Locking at High Concentrations

As the concentration increases to 0.008%, the magneto-optical response exhibits significant nonlinear distortion. The down-sweep slope decays to -0.0031 ($R^2 = 0.8394$), while the up-sweep slope drops to -0.0000 ($R^2 = 0.0002$). The reduced slope confirms the "Concentration Quenching" effect: reduced interlayer spacing at high concentrations enhances magnetic dipole coupling, suppressing the rotation efficiency of monomeric magnetic moments.The disappearance of the up-sweep response is attributed to "Structural Locking." While recent studies have achieved reversible magnetic alignment of GO in specific ferrofluidic matrices [9], our results indicate that in pure high-concentration dispersions, dense nanosheets tend to form stable liquid-crystalline domains [10]. In this regime, the external restoring torque is insufficient to overcome the significant yield stress and steric hindrance arising from the strong gel network [11]. Consequently, the orientation becomes effectively "frozen," causing the sensor to lose the linear tracking capability required for dynamic magnetic field monitoring. Fig.6 is the linear fitting analysis of the intrinsic magneto-optical response (θ_{GO}) versus magnetic flux density (B) at a concentration of 0.008%.

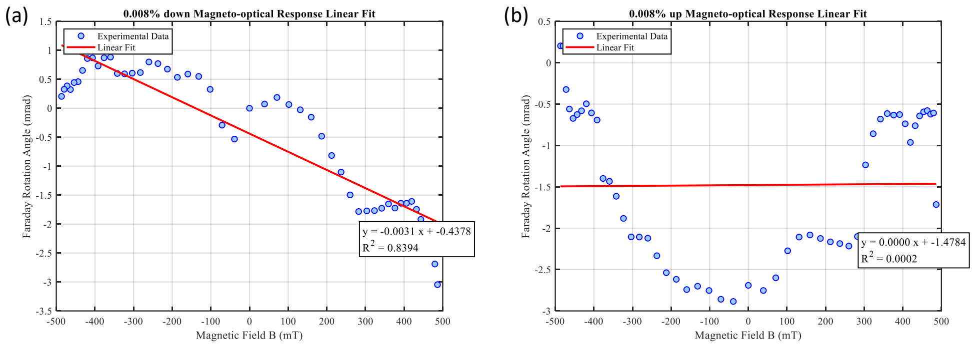

Fig. 6. Fitting Comparison of $\theta_{GO} - B$ at 0.008%

4.3.3 Instability Analysis of Transitional State

The 0.005% concentration group exhibits extremely low linearity (Down $R^2 = 0.4823$,Up $R^2 = 0.2472$) and unstable slopes (-0.0015 vs 0.0011). This indicates that the concentration lies within a "Rheological Critical Zone", transitioning from monomeric free response to collective interaction. The lack of dynamic equilibrium among Brownian motion, magnetic torque, and interlayer interference results in chaotic response patterns, further highlighting the uniqueness of the 0.0029% group as a physical limit analysis point. Fig.7 is the linear fitting analysis of the intrinsic magneto-optical response (θ_{GO}) versus magnetic flux density (B) at a concentration of 0.005%.

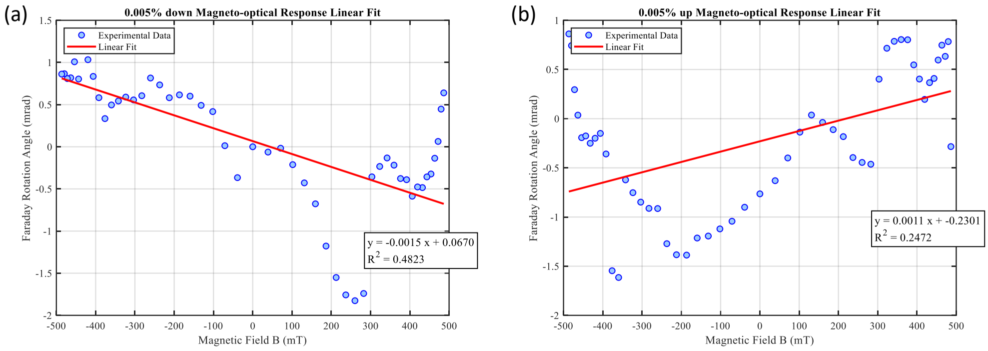

Fig. 7. Fitting Comparison of $\theta_{GO} - B$ at 0.005%

4.4 Dynamic Response and Hysteresis Evaluation

This section evaluates the dynamic reliability of the sensor via quasi-static cyclic scanning ($5A \rightarrow -5A \rightarrow 5A$).

4.4.1 Quantitative Characterization of Hysteresis Error

For the optimal concentration of 0.008%, the Full Scale Output (FSO) is measured at approx. 8.98mV. A comparison between "Up-sweep" and "Down-sweep" data reveals a maximum voltage deviation of 0.59mV near the zero point, yielding a maximum "Hysteresis Error" of approx. 6.57%.Results indicate that despite certain kinetic lag in the liquid medium, the error level is controllable with stable response envelopes, verifying the feasibility for low-frequency current monitoring.

4.4.2 Physical Attribution of Hysteresis Mechanisms

The formation of hysteresis loops reflects the dynamic interplay between macroscopic excitation and microscopic resistance, attributed to two main factors:

1.Relaxation Lag due to Solvent Viscosity: The high-viscosity glycerol matrix induces significant "Viscoelastic Relaxation". GO nanosheets must overcome immense fluid drag during orientation, causing the rotational evolution to lag behind magnetic field changes, thereby forming a macroscopic closed loop on the $\Delta V - B$ plot.

2.Steric Hindrance at High Concentrations: At 0.008%, reduced interlayer spacing enhances "Steric Hindrance". Mechanical friction and dynamic aggregation among dense nanosheets increase the structural barrier for magnetic moment restoration, further impeding linear recovery during demagnetization.

This chapter establishes a comprehensive framework from signal demodulation to performance evaluation. First, the "Differential Baseline Subtraction" algorithm successfully isolated background interference, defining the "Negative Magneto-optical Effect" of GO and measuring a specific Verdet constant as high as $1.72 \times 10^4 \text{rad}/(\text{T} \cdot \text{m})$ in ultra-dilute solutions, confirming its superior conversion efficiency. In terms of engineering optimization, the 0.008% concentration group was found to maintain the highest sensitivity of $-0.00391\text{mV}/\text{mT}$ while controlling hysteresis error at 6.57%, effectively overcoming the massive 34.08% error observed in the low-concentration group (0.0029%) due to instability. This achieves an optimal balance between SNR and dynamic reliability. Furthermore, the mechanisms of "Concentration

Quenching" and "Structural Locking" at high concentrations were explored, revealing the orientational dynamics of nanosheets in viscous fluids and providing a solid theoretical basis for sensor design.

5 Conclusion

To address bottlenecks such as saturation in traditional CTs and stress birefringence in solid OCS, this study proposes a liquid magneto-optical sensing scheme based on GO dispersion. The work encompasses theoretical modeling, system construction, and algorithm optimization, establishing a concentration-sensitivity mapping model. The detection system was optimized using a "Near-extinction Bias Strategy" and 3rd-order nonlinear reconstruction, while high-fidelity intrinsic signal extraction was achieved via "Differential Baseline Subtraction" and normalized inversion algorithms.

Experiments validated the significant "Negative Magneto-optical Effect" of GO. At an ultra-dilute concentration of 0.0029%, the Verdet constant reached $0.5\mathrm{rad}/(\mathrm{T}\cdot\mathrm{m})$, demonstrating superior intrinsic efficiency. Through trade-off evaluation, 0.008% was identified as the optimal engineering concentration, achieving a peak sensitivity of $0.00391\mathrm{mV}/\mathrm{mT}$, linearity exceeding 0.98, and controlled hysteresis of 6.57%, effectively resolving the massive 34.08% error caused by Brownian motion in the dilute group. Furthermore, mechanisms of "Concentration Quenching" and "Structural Locking" at high concentrations were elucidated, clarifying the impact of viscous drag and steric hindrance on dynamic response.

This project realizes innovations across three key dimensions. First, regarding mechanism, it exploits liquid isotropy to fundamentally eliminate stress birefringence interference. Second, in terms of methodology, composite algorithms are constructed to mitigate high optical absorption and parasitic effects inherent to liquid media. Finally, for engineering design, concentration tunability is leveraged to overcome the fixed Verdet constant of solid crystals, enabling programmable sensitivity. To meet practical grid deployment demands, future work will focus on establishing temperature compensation models for glycerol viscosity to enhance all-weather stability, exploring miniaturization via microfluidics or micro-structured fibers, and optimizing dynamic tracking speed under high-current pulses to achieve high-fidelity reconstruction of transient fault waveforms.

References

[1] Sun, H.; Huang, S.; Peng, L.: High-Current Sensing Technology for Transparent Power Grids: A Review. Vol. 5, pp. 326–358. IEEE Open Journal of the Industrial Electronics Society, (2024)

[2] Costa, M. M.; Martinez, M. A. G.; Costa, J. C. W. A.: Review of Uncertainty Sources in Optical Current Sensors Used in Power Systems. Vol. 17, 4162. Energies, Basel, Switzerland (2024)

[3] Chen, Y. X.; Sun, J.; Meng, B. Q.: Recent development of optical electric current transformer and its obstacles. arXiv:2412.06282. arXiv, (2024)

[4] Amiolemen, A.; Fusiek, G.; Niewczas, P.: Towards the Development of a Photonic Current Sensor for HVDC Networks. 2024 IEEE International Instrumentation and Measurement Technology Conference (I2MTC). IEEE, Glasgow, United Kingdom (2024)

[5] Mandl, J. M.; Trampitsch, P. P.; Schachinger, P.; Albert, D.; Klambauer, R.; Bergmann, A.: Development of a fiber optic current sensor for low DC measurements in the power grid. Vol. 73, 1502908. IEEE Transactions on Instrumentation and Measurement, (2024)

[6] Wei, Y.; Niu, G.; Xue, Y.; Xu, Y.; Luo, B.; Jiang, C.: Optical Fiber Vector Magnetic Field Sensors Based on Magnetic Fluid: A Review. Vol. 24, pp. 28538–28552. IEEE Sensors Journal, (2024)
[7] Lan, T.; Ding, B.; Liu, B.: Magneto-optic effect of two-dimensional materials and related applications. Vol. 1, pp. 298–310. Nano Select, Weinheim, Germany (2020)
[8] Carothers, K. J.; Norwood, R. A.; Pyun, J.: High Verdet Constant Materials for Magneto-Optical Faraday Rotation: A Review. Vol. 34, pp. 2531–2544. Chemistry of Materials, (2022)
[9] Xu, Y. T.; Ackroyd, A. J.; Momeni, A.; Oudah, M.; MacLachlan, M. J.: Magnetic field-responsive graphene oxide photonic liquids. Vol. 9, pp. 317–322. Nanoscale Horizons, London, UK (2024)
[10] He, H.; Guan, L.; Le Ferrand, H.: Controlled local orientation of 2D nanomaterials in 3D devices: methods and prospects for multifunctional designs and enhanced performance. Vol. 10, pp. 19129–19168. Journal of Materials Chemistry A, London, UK (2022)
[11] Lei, Y.; Boucenna, I.; Thévenet, V.; Brett, W.; Paineau, E.; Ponton, A.: The Rheological and Structural Properties of Aqueous Graphene Oxide Dispersions: Concentration and pH Dependence. Vol. 40, pp. 16048–16057. Langmuir, Washington, DC, USA (2024)